RESEARCH ARTICLE

WILEY

Fragility curves and seismic demand hazard analysis of rocking walls restrained with elasto-plastic ties

Fabio Solarino[1,2] ⓘ　|　**Linda Giresini**[3] ⓘ

[1] ISISE, Institute of Science and Innovation for Bio-Sustainability (IB-S), Department of Civil Engineering, University of Minho, Guimarães, Portugal

[2] Department of Energy, Systems, Territory and Constructions Engineering (DESTEC), University of Pisa, Pisa, Italy

[3] Department of Civil and Industrial Engineering (DICI), University of Pisa, Pisa, Italy

Correspondence
Fabio Solarino, ISISE, Institute of Science and Innovation for Bio-Sustainability (IB-S), Department of Civil Engineering, University of Minho, Guimarães, Portugal.
Email: f.solarino1@studenti.unipi.it

Present Address: Fabio Solarino, Largo Lucio Lazzarino, 1, 56126, Pisa (PI), Italy

Funding information
Portuguese Foundation for Science and Technology (FCT), Grant/Award Number: SFR/BD/131652/2017; European Social Fund

Abstract

The dynamic stability of out-of-plane masonry walls can be assessed through non-linear dynamic analysis (rocking analysis), accounting for transverse walls, horizontal diaphragms and tie-rods. Steel tie-rods are widely spread in historical constructions to prevent dangerous overturning mechanisms and can be simulated by proper elasto-plastic models. Conventionally, design guidelines suggest intensity-based assessment methods, where the seismic demand distribution directly depends upon the selected intensity measure level. Fragility analysis could also be employed as a more advanced procedure able to assess the seismic vulnerability in a probabilistic manner. The boundedness of this approach is herein overcome by applying a robust stochastic seismic performance assessment to obtain seismic demand hazard curves. A sensitivity study is carried out to account for the influence of wall geometry, the minimum number of seismic inputs, and the mechanical parameters of tie-rods. Fragility analysis, prior to seismic demand hazard analysis is applied on over 6000 analyses, revealing that intensity measures are poorly correlated both for 1-D and 2-D correlation, hardly leading to the selection of the optimal intensity measure. The tie-rod ductility, followed by its axial strength and wall size, is the mechanical parameter mostly influencing the results, whereas the wall slenderness does not play a significant role in the probabilistic response.

KEYWORDS
elasto-plastic tie-rods, fragility curves, rocking, seismic demand hazard curves

1　|　INTRODUCTION

The seismic vulnerability of out-of-plane masonry walls can be investigated through the rocking analysis, allowing for dynamic nonlinear time-history analysis of rigid blocks tilting on their base.[1–4] Such a methodology requires the mechanism to be defined a priori and is aligned with the kinematic approach[5] widely spread among the research community and practitioners. The rocking analysis can be seen, in fact, as the natural improvement of the pseudo-static methodology as allows to account for complex dynamic effects, even when the maximum static capacity is attained. In the pioneering Housner's work,[6] rocking analysis was first systematized; in it, sliding and bouncing are neglected for sufficiently slender
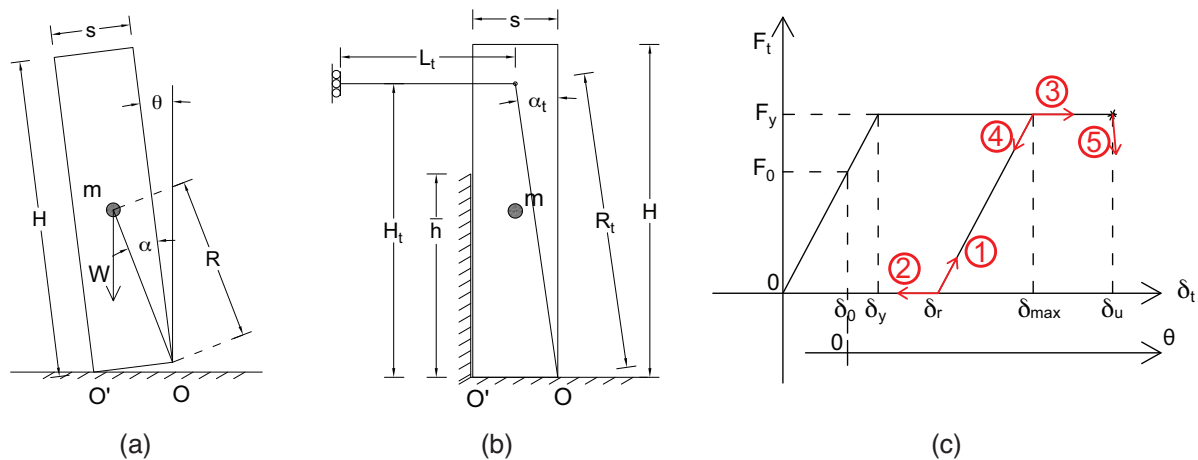
FIGURE 1 (a) Free-standing (b) restrained rocking blocks. (c) Elasto-plastic constitutive model assumed for the steel tie-rod

blocks (i.e., $\lambda \geq 5$).[7] Moreover, the energy is dissipated through a coefficient of restitution, solely function of the block geometry, $e_H = 1 - \frac{3}{2}sin^2(\alpha)$, where $\alpha = \tan^{-1} s/H$, being s and H the wall thickness and height, respectively (Figure 1a), valid for slender blocks. The velocity reduction factor was experimentally calibrated to be about $95\% \, e_H$ for unreinforced masonry walls in one-sided motion.[8]

Recently, the equation of motion was improved in order to account for different restraints and boundary conditions, such as the presence of horizontal diaphragms,[9] transverse walls, roof thrusts,[10] steel tie-rods,[11] or tendons[12] and dissipative devices.[13] The influence of the tie-rods on the rocking motion mainly depends on their ultimate elongation and strength. Moreover, if one deals with historical tie-rods, the mechanical properties can be scattered, as shown by Calderini et al.[15] The tie-rods strongly reduce the mean values of maxima amplitude rotations, as demonstrated by Casapulla and Argiento[16] also for non-linear static analyses. The effect of the change of aspect ratio of two walls of the same size was shown to be negligible for tied walls.[17] The same occurred for walls restrained by tie-rods at different heights; the overall effect of tie-rod length (normalized to the wall thickness and variable between 4 and 20) as well as the normalized prestress (between 0 and 0.6) is limited. As for the influence of mechanical properties, the role of the elastic modulus and of the axial stiffness appeared to be negligible. The yield strength is the most relevant parameter that influences the response, besides the brittle or ductile behavior of the tie-rod. Unfortunately, all these conclusions are drawn from the results of deterministic analyses, performed for a specific seismic scenario, and for a single level of intensity. The results are seldom computed in terms of percentile or simply mean value, resulting not fully reliable. For these reasons, the seismic vulnerability of restrained rocking blocks is made in this paper through a more sophisticated probabilistic procedure.

As well known, the seismic vulnerability can be computed as the probability for a certain component or a global structure of exceeding a certain limit state, defined in terms of a representative engineering demand parameter (EDP), and can be shown through the construction of fragility curves (FC) conditional to the selected intensity measure (IM).[18] By definition, this approach is conditional to the IM, meaning that the capacity obtained for one IM differs from another calculated for a different IM. The latter intensity-based method is however conditional to the selected IM and does not account for the annual likelihood that a certain level of the seismic demand will be exceeded.

A more robust procedure is the methodology recommended by Bradley,[19] which provides the rate of exceedance of various seismic demand values in the form of the so-called seismic demand hazard curve (SDHC). The latter is obtained by integrating the distribution of the demand over multiple intensity levels based on the site seismic hazard, thus quantifying the likelihood that a certain limit state will be exceeded over the structure lifetime. To the authors' knowledge, this is the first time that such a procedure is applied to the vulnerability of free or restrained rocking blocks and particularly of masonry walls.

In this perspective, this paper examines the influence of tie-rod resistance and ductility on the dynamic stability of restrained rocking blocks simulating rigid-like out-of-plane mechanisms frequently observed in historical masonry constructions. Based on the distribution of seismic response analysis data, a sensitivity analysis is carried out for different geometric and mechanical parameters, discretely defined within reasonable ranges. The equation of motion is firstly introduced in Section 2, while in Section 3 the reference sample geometry is presented, followed by the definition of

the probabilistic models. The main parametric analysis results are shown in Section 5 and relevant outcomes are finally discussed in Section 6.

2 | DYNAMICS OF RESTRAINED ROCKING BLOCKS

Based on the leading formulation originally suggested by Housner,[6] the equation of motion of laterally restrained rigid block tilting around the base corners reads (Figure 1b):

$$I_0\ddot{\theta} + sgn(\theta)mgR \sin A_\theta + T_t + T_L = m\ddot{u}_g R \cos A_\theta \tag{1}$$

The term in the right hand side refers to the seismic excitation: $m\ddot{u}_g$ is the seismic effective force applied to the block of size R and slenderness α ($\tan^{-1}(s/H)$). The argument of the cosine is:

$$A_\theta = \alpha - sgn(\theta)\,\theta \tag{2}$$

The first term in the left-hand side of Equation (1) refers to the inertia force ($I_0 = 4/3\, m\, R^2$, polar inertia moment around the pivot point O), the second one relates to the self-weight $m\,g$ which acts as stabilizing term as long as the projection of the gravitational force falls into the wall thickness. The term T_t of Equation (1) refers to the contribution given by the tie-rod, whose role is modeled as individual elasto-plastic horizontal restraint only acting for outward rotations ($\theta \geq 0$):

$$T_t = sgn(\theta)K\beta^2 R^2 \cos A_{t,\theta}[\sin \alpha_t - \sin A_{t,\theta}] \tag{3}$$

in which K is the spring stiffness, $A_{t,\theta} = \alpha_t - sgn(\theta)\,\theta$, where α_t is a position angle dependent on the position coefficient $\beta = R_t/R$. The elongation strain ϵ of the tie-rod of length L_t due to its elasticity is equal to $\frac{F}{EA}$, where F is the axial force in the tie-rod and EA/L_t its axial stiffness. The tie displacement depends on the rotation:

$$u_t = R_t[\sin \alpha_t - \sin A_{t,\theta}] \tag{4}$$

When a pre-stress force F_0 is applied to the tie-rod, the latter endures an additional elongation $\epsilon_0 = \frac{F_0}{KL} = \frac{F_0 L_t}{EAL}$. Considering Equation (4), the potential energy V stored by the tie-rod is:

$$V = \frac{1}{2}K(u_t + \epsilon_0 L)^2 = \frac{1}{2}K\left[R_t(\sin \alpha_t - \sin A_{t,\theta}) + \frac{F_0}{K}\right]^2 \tag{5}$$

The derivation of the potential energy with respect to the variable θ gives the elastic term T_t of Equation (3):

$$T_{t,e} = \frac{\partial V}{\partial \theta} = \left[sgn(\theta)KR_t(\sin \alpha_t - \sin A_{t,\theta}) + F_0\right]R_t \cos A_{t,\theta} \tag{6}$$

The modeling of elasto-plastic phases of the tie-rod depends on the tie-rod elongation history or, equivalently, on its displacement from a reference value, δ_t. Five cases are distinguished as shown in Figure 1c: (1) from inactive to elastic, $\delta_t > \delta_r$; (2) from elastic to inactive, $\delta_t < \delta_r$; (3) from elastic to plastic, $\delta_t > \delta_{max}$; (4) from plastic to elastic, $\delta_t < \delta_{max}$; and (5) rupture, $\delta_t > \delta_u$. Once yielding is attained, the spring exerts the constant force F_y. The term related to the tie contribution is then:

$$T_{t,p} = sgn(\theta)F_y R_t \cos A_{t,\theta} \tag{7}$$

In summary, the complete equation of motion is given in Equation (1), where the T_t term assumes either the value expressed in Equation (6) or that of Equation (7). Alternatively, one of the two terms $T_{t,e}$ and $T_{t,p}$ is recalled by the MATLAB code through a specific subroutine depending on the actual value of the tie-rod displacement δ_t.

The tie-rod influence can be controlled through the following parameters: stiffness, yielding, ductility and strength associated to it. T_L has a similar meaning but refers to the lateral walls modeled as elastic spring bed. Its contribution is

TABLE 1 Reference sample geometry and seismic parameters

Description	Symbol	Value	Unit	Description	Symbol	Value	Unit
Wall slenderness	H/s	10	-	Normalized pretension force	f_0/f_y	50	%
Wall thickness	s	0.60	m	Soil factor	S	1.1461	-
Wall length	L	1.00	m	Period of the first mode shape	T_1	0.32	s
Masonry specific weight	γ	19	kN/m³	Modal mass participation factor	e^*	1	-
Coefficient of restitution	e	0.985	-	Confidence factor	CF	1	-
Masonry Young's modulus	E_m	690	MPa	Behavior factor	q	1	-
Effective lateral wall length	L_{eff}	1.20	m	Peak ground acceleration (ULS)	$a_{g,ULS}$	0.278	g
Steel Young's modulus	E_s	210	GPa	Equivalent viscous damping ratio	ξ_1	5	%
Yield stiffness	f_y	235	MPa	Modal participation factor	γ_1	1.5	-
Ultimate elongation	ϵ_u	10	%	Mode shape	ψ_1	0.5	-
Tie position	H_t	6 (= H)	m	Maximum floor acceleration	$a_{z,1}$	0.44	g
Tie length	L_t	10 s	m	Design load multiplier	α_0	0.44	-

different from zero only for inward rotations (spring bed in compression, Figure 1b). T_L is function of the rotation angle θ, the stiffness of the spring bed K_L, the effective height of the spring bed $\bar{h}$ and the block thickness s[9]:

$$T_L = sgn(\theta)K_L\bar{h}\left(A + \frac{B\bar{h}}{2} + \frac{C\bar{h}^2}{3}\right) \quad (8)$$

where:

$$A = sgn(\theta)s^2 \sin\theta \cos\theta(1 - \cos\theta)$$

$$B = s\left(\sin^2\theta \cos\theta - \cos^3\theta + \cos^2\theta\right) \quad (9)$$

$$C = sgn(\theta)\sin\theta \cos^\theta$$

The stiffness of the spring bed K_L can be calculated as function of the horizontal elastic modulus of masonry E_L, effective transverse wall length L_{eff} and transverse wall thickness t_t as illustrated in Giresini and Sassu.[9]

3 | GEOMETRIES AND ASSUMPTIONS

3.1 | Wall geometries and energy dissipation parameters

The reference sample employed for the parametric analysis performed herein is aimed at simulating an unreinforced masonry wall portion at the top-level of historical constructions, usually highly vulnerable to seismic shakes. The wall slenderness (H/s) should also be consistent with the assumption of rigid out-of-plane mechanism. Indeed, it was seen that complex multi degree-of-freedom mechanisms may arise for values of $H/s > 12$.[20] Let us define the reference geometry as rectangular wall with unit length, slenderness $H/s = 10$, and thickness $s = 0.6m$, adjacent to transverse walls and restrained by $L_t = 10s$ length elasto-plastic ties with diameter derived by Equation (10) (Table 1). Setting this geometry and boundary conditions, it is possible to change the remaining influencing parameters. In order to study both the role of block geometry (in terms of **aspect ratio** and **scale effect**), the **ductility** and the **tie resistance**, the influencing parameters are selected as depicted in Table 2 within reasonable ranges.

The rectangular wall is assumed to have unitary width, specific weight of $\gamma = 19$ kN/m³, and no openings. The block tilts around the pivots placed at the corners, O and O' (Figure 1), neglecting possible eccentricity due to masonry crushing. This hypothesis is supported by high uncertainty on material mechanical characteristics, in fact leading to uncertain position of the real hinge. The energy is assumed to be solely dissipated at the impacts through the analytical coefficient of restitution (COR) proposed by Housner, unless otherwise specified. More details about the COR values adopted for one-sided rocking are given in Section 5.1. The presence of orthogonal walls is taken into account adopting a bed of springs equally distributed

TABLE 2 Definition of influencing parameters and corresponding parameter values

Aspect under study	Description	Symbol	Assumed parameter values[a]	Unit
Aspect ratio	Block slenderness	H/s	$8 \div \mathbf{10} \div 12$	[-]
Scale effect	Block thickness	s	$0.30 \div \mathbf{0.60} \div 0.90$	[m]
Tie ductility	Ultimate steel strain	ϵ_u	$0 \div \epsilon_y \div 2 \div \mathbf{10} \div 20$	[%]
Tie resistance	Steel yielding stress	f_y	$142 \div \mathbf{235} \div 294$	[MPa]

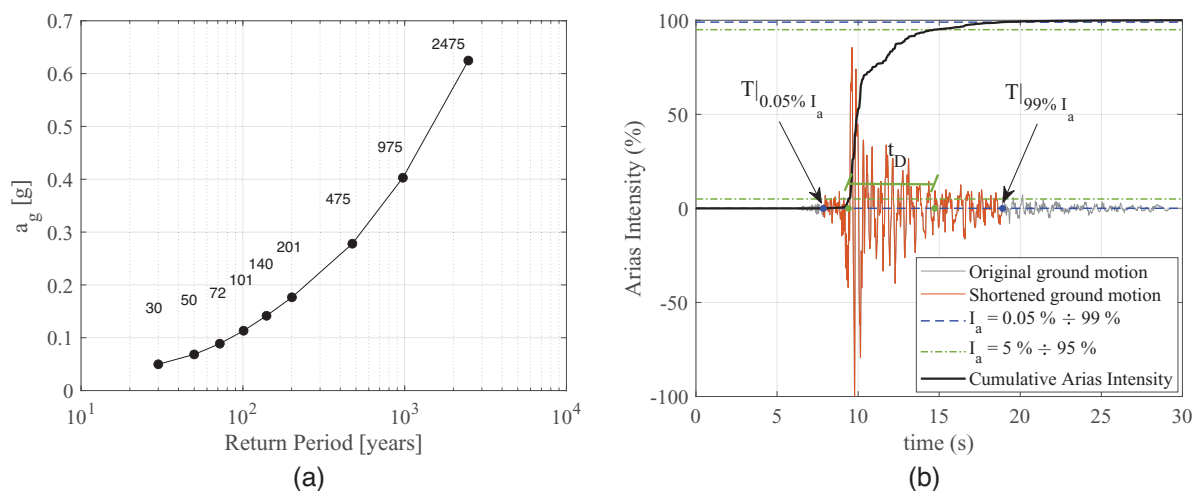[a]In bold values correspond to the reference geometry.

FIGURE 2 (a) Seismic hazard curve of the selected site (Carlentini - Sicily); (b) Reduced strong motion duration

along the whole height of the wall, hence simulating an elastic impact. The lateral stiffness (Equation 8) can be assumed as $K_L = E_L \, s/L_{eff}$,[9] function of the masonry Young's modulus, $E_L = 690$ MPa valid for rubble stone masonry (Tab C8.5.I, NTC2018[21]), transverse wall thickness, s and effective length, $L_{eff} = 1.2$ m.

An elastic-perfectly plastic constitutive model is assumed for the steel tie placed on top of the wall ($H_t = H$, Figure 1b). The material model assumes elastic unloading and residual strain, hence defining five possible events within the nonlinear stress state of the tie (Figure 1c, see also Section 2). A modern steel S235 class is considered having yielding stiffness $f_y = 235$ MPa, ultimate elongation $\epsilon_u = 10\%$, and elastic modulus, $E_s = 210$ GPa (Table 1).

3.2 | Steel tie-rod design

The minimum tie-rod diameter is designed for the serviceability limit state, SLS, according to the simplified force-based approach suggested by the commentary to the Italian standard.[21] The mechanism is assumed not to take place at the foundation level, hence including an amplification factor accounting for unfavorable dynamic effects, and setting a unitary behavior factor. The building is supposed located at the most seismically vulnerable site in Italy (Carlentini, Sicily) for which the seismic hazard curve is shown in Figure 2a. The minimum design value of steel tie area reads:

$$A_{s,min} = \frac{F_{t,min}}{50\% f_y} \tag{10}$$

assuming the pre-tensional state equal to $50\% f_y$, as suggested by Tomaževič[23] in order to better exploit the whole ductile capacity of the anti-seismic device. Despite the actual tie-rod area should be rounded compatible with available standard diameters, for the purpose of this work, the minimum value of tie-rod area is set in order to keep the geometrical correlation with the geometry and to be on the safe side. The tie force $F_{t,min}$ at the numerator of Equation (10) refers to the minimum horizontal force applied at the level of the tie in order to guarantee the equilibrium of the block subject to the equivalent

TABLE 3 Definition of the selected limit states LS

	Definition	EDP (LS)	Damage level
LS_0	Rocking initiation	$\theta/\alpha = 10^{-4}$	Uplift
LS_1	Limited rocking	$\theta/\alpha = 0.1$	Negligible damage
LS_2	Moderate rocking	$\theta/\alpha = 0.4$	Minor damage
LS_3	Severe rocking	$\theta/\alpha = 1.0$	Severe damage
LS_4	Near collapse	$\theta/\alpha = 1.5$	Possible overturning

horizontal seismic force (acting at the center of gravity) given by the load multiplier α_0,

$$F_{t,min} = \frac{W}{2H_t}(\alpha_0 H - s); \quad \alpha_0 = \frac{a_{Z,1}\, e^*\, CF}{q\, g} \tag{11}$$

where W is the block self weight, $a_{Z,k}$ is the maximum floor acceleration at height, Z, $e^* = 1$ is the modal mass participating factor, $CF = 1$ is the confidence factor, $q = 1$ is the behavior factor and g is the gravity acceleration. The amplified acceleration reads[24]:

$$a_{z,1} = S_e(T_1, \xi_1)|\gamma_1 \psi_1(Z)|\sqrt{1 + 0.0004\xi_1^2} \tag{12}$$

where, $S_e(T_1, \xi_1)$ is the elastic base spectral acceleration function of the characteristic of the soil and dynamic parameters of the building, assumed to have $\xi = 5\%$ equivalent viscous damping and the first period of vibration simply assumed as $T_1 = 0.05 H_b^{3/4}$, according to equation C7.3.2 of the same guidelines. $\gamma_1 = 3n/2n + 1$ is the modal participation factor of the building with n floors, and $\psi_1 = Z/H_b$ is the value of the modal shape at height Z. The main geometrical and seismic parameters of the reference sample are summarized in Table 1.

4 | DEFINITION OF THE ASSESSMENT PROCEDURES

Two seismic assessment procedures are adopted herein with the common aim of studying the influence of elasto-plastic restraints in the seismic vulnerability of masonry walls rocking out-of-plane: (i) fragility analysis[25,26]; (ii) seismic demand hazard analysis.[19] Both procedures are based on a lognormal distribution of response data, which is a common but not unique assumption, widely used by several authors.[26–29] The first one can be denoted as probabilistic model able to produce univariate and multivariate FC in the form of probability level (from 0 to 1) of occurrence of a given event. The second one can be considered as the step forward with respect to the previous and is referred to as a stochastic procedure in the sense that it allows for evaluation over the time of a random variable. Indeed, the output of such a procedure is the annual exceedance rate of a certain LS in terms of EDP. It is worth noting that geometrical and mechanical parameters are changed discretely (Table 2) to carry out a sensitivity analysis, whereas only the seismic response analysis results are treated statistically. This section firstly presents the definition of EDP and the loading protocol, common to both procedures, then the latter are briefly summarized, referring to cited literature for a detailed description.

4.1 | Engineering demand parameter and limit states

The definition of the EDP is requested for any statistical procedure, therefore the maximum normalized rotation, (θ_{max}/α) is adopted here, as the best seismic performance parameter. Five LS are defined in terms of EDP, aligned with Giresini et al.[18] and Dimitrakopoulos and Paraskeva[25] (Table 3). The rocking initiation LS_0 could also be defined by the minimum horizontal load multiplier necessary to disturb the static equilibrium, α_0, as defined in Section 3, Equation (11), meaning that for free blocks only accelerograms with PGA > $a_{min} = s/H$ g could in principle cause uplift. However, numerical evidences show that several restrained samples have zero rotations even for higher values of PGA, because of the positive effect of tie pretension and of the lateral wall support. Conversely, one single threshold parameter can be defined in terms of normalized rotation, $\theta/\alpha = 10^{-4}$, since lower values result in negligible movements.

TABLE 4 Amplified accelerations (in g) of the seismic ground motion hazard considered for the response analyses of 6 IM levels

Return period [years]	RP	101	140	201	475	975	2475
Peak ground acceleration	PGA	0.11	0.14	0.18	0.28	0.40	0.62
Amplified floor acceleration	PGA_Z	0.18	0.22	0.28	0.44	0.63	0.98

TABLE 5 Strong motion waveform retrieved from ESM database[30]

| ID	Date [yyyy/mm/dd]	Time [hh:mm]	Station code [SSS]	Direction [DD[a]]	Site -	M_L [-]	PGA [g]	PGV [cm/s]
1	2016/08/24	01:36	AMT	WE	Accumoli	6.0	0.87	43.55
2	2016/08/24	01:36	NRC	NS	Accumoli	6.0	0.37	29.75
3	2016/08/24	02:33	FOC	WE	Norcia	5.4	0.18	2.79
4	2016/08/24	02:33	NRC	NS	Norcia	5.4	0.19	9.80
5	2016/08/26	04:28	AMT	NS	Amatrice	4.7	0.34	11.00
6	2016/08/26	04:28	PCB	NS	Amatrice	4.7	0.31	5.50
7	2016/10/26	17:10	CMI	WE	C.S.A. sul Nera	5.4	0.72	55.70
8	2016/10/26	17:10	CNE	WE	C.S.A. sul Nera	5.4	0.56	17.34
9	2016/10/26	19:18	CMI	WE	Visso	5.9	0.65	43.76
10	2016/10/26	19:18	FOC	WE	Visso	5.9	0.62	20.00
11	2016/10/30	06:40	MZ24	WE	Norcia	6.1	1.02	73.60
12	2016/10/30	06:40	MZ51	NS	Norcia	6.1	0.96	74.98
13	2016/11/01	07:56	MMO	NS	Visso	4.7	0.19	7.58
14	2016/11/01	07:56	RQT	WE	Visso	4.7	0.13	2.80
15	2016/11/03	00:35	PBN	NS	P. Torina	4.8	0.31	8.47
16	2016/11/03	00:35	T1219	WE	P. Torina	4.8	0.34	7.88
17	2017/01/18	09:25	AMT	NS	Capitignano	5.4	0.35	13.15
18	2017/01/18	09:25	PCB	NS	Capitignano	5.4	0.18	3.79
19	2017/01/18	10:14	AMT	NS	Capitignano	5.4	0.32	16.10
20	2017/01/18	10:14	PCB	NS	Capitignano	5.4	0.60	21.02
21	2017/01/18	10:25	MSCT	NS	Montereale	5.3	0.28	17.03
22	2017/01/18	10:25	PCB	NS	Montereale	5.3	0.56	19.35
23	2017/01/18	13:33	MSCT	NS	C. Amiterno	5.1	0.16	6.27
24	2017/01/18	13:33	PCB	NS	C. Amiterno	5.1	0.29	5.55
25 - 48	records [51 - 74], Table 5 in Giresini et al. 2018[18]					> 5.5	var	> 45

[a]DD: earthquake direction: North-South, NS; West-East, WE.

4.2 | Loading protocol

A selection of 48 natural waveforms is performed from the Engineering Strong Motion Database,[30] 24 of which belong to seismic events that stroke Central Italy between 2016 and 2017, while additional 24 seismic records are selected as characterized by high PGV value (> 45 cm/s). The list of accelerograms is shown in Table 5 along with corresponding seismic parameters. Each set of the 48 natural ground motions is then scaled to 6 IM levels (see Table 4) and used in both positive and negative direction, given the asymmetry of the problem, thus leading to $48 \times 2 \times 6 = 576$ NLTH analyses performed for each block sample. That number, multiplied by 11 samples lead to more than 6000 analyses in total. Within the aim of this work, PGA levels are selected within a return period range of 101 < RP < 2475 years corresponding to the site with highest seismic hazard in Italy (Carlentini, Sicily), whose hazard curve is shown in Figure 2a. The accelerations are amplified to consider the mechanism to occur at the second floor of a residential building through the factor $a_{Z,1}/(q\, a_{g,SLV}) = 1.57$, leading to the amplified hazard curve whose values are schematically summarized in Table 4.

Giving the high computational effort, a reduced strong motion duration is considered for the analysis as the period between 0.05% and 99% of the total Arias intensity I_a (Figure 2b). This is defined as the cumulative energy per unit weight

FIGURE 3 Rocking probability tree highlighting the computation of the final probability of exceeding a given capacity (adapted from [25])
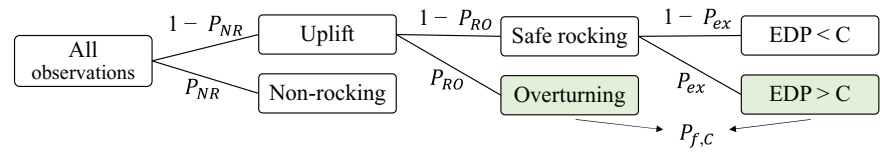
absorbed by an infinite set of undamped single-degree-of-freedom oscillators at the end of an earthquake,

$$I_a = \frac{\pi}{2g} \int_0^{T_f} a_x^2(t)dt \tag{13}$$

Although Trifunac and Brady[31] suggest 5% and 95% values as thresholds defining the period of interest (significant duration, t_D), a wider domain is considered herein in order not to neglect relevant portions of the strong motion. Fifteen total IM_s are evaluated for each waveform related to acceleration, velocity and integral spectral, whose expressions can be found in Giresini et al.[18]

4.3 | Fragility analysis and rocking probability tree

The following procedure, thoroughly described in Dimitrakopoulos and Paraskeva,[25] Psycharis et al.,[32] and Baker,[26] aims at calculating the conditional probability, $P_{f,C}$ that the rocking block exceeds a certain capacity limit ($EDP > C$), for a given IM and gives an estimation of the most efficient IM, starting from dynamic structural analysis results. Indeed, the selection of the optimal IM is not trivial but fundamental for the effectiveness of the final curves.[33] Actually, it is of paramount relevance to adequately handle both non-rocking (NR, i.e., $\theta/\alpha < 10^{-4}$) and overturning (RO) cases, since results may be strongly affected by them. Potentially, both NR and RO can simply be excluded from fragility analysis neglecting part of result data. There are mainly two drawbacks after such a strong assumption: (i) in case many samples do not even uplift (or in case they overturn), the dataset is strongly reduced; (ii) if an earthquake leads to RO or NR of one sample, the same ground motion should be excluded for any other sample, thus possibly eliminating several meaningful data. In order to properly handle both NR and RO, an accurate methodology, described in Baker[26] is combined to the one suggested by Dimitrakopoulos and Paraskeva,[25] involving the separate computation of the probability of non-rocking P_{NR}, and probability of overturning, in case the block uplifts P_{RO}. These *categorical* probabilities are later merged with the probability of exceeding a given intermediate capacity, given that the block uplift and given that it does not overturn, P_{ex}. Denoting the probability of uplift, $P_{UP} = 1 - P_{NR}$, the rocking probability tree of Figure 3 graphically guides to the calculus of the final probability, $P_{f,C}$ as:

$$P_{f,C} = P_{UP}[P_{RO} + (1 - P_{RO})P_{ex}] \tag{14}$$

Assuming a log-normal distribution for the "safe rocking" response data, SR (i.e., $10^{-4} < \theta/\alpha \leq 1.5$), it is possible to estimate the probability that the rocking block exceeds a certain capacity, C, conditioned to a given IM, given that the block uplifts but does not overturn P_{ex} as:

$$P_{ex}(EDP \geq C|IM) = 1 - \Phi\left(\frac{\ln(C/S_D)}{\beta_{D|IM}}\right) \tag{15}$$

where $\Phi(\cdot)$ is the standard normal cumulative distribution function (CDF), and $\beta_{D|IM}$ is the standard deviation (or dispersion) of the logarithm of the demand conditioned on the IM. Assuming an exponential relationship between the median seismic demand, S_D and the IM, $S_D = a\,IM^b$; a and b are regression coefficients that can be obtained after linear regression of the logarithms of the IM considering SR response data.

Overturning and uplift probabilities differ from the probability of exceedance for the *categorical* characteristic of the observations: the block can, in fact, overturn or not and, similarly, it can uplift or not, thus implying different methods for fragility function fitting (Figure 3). The method adopted herein refers to the multiple stripes analysis approach (MSA) described in Baker[26] aimed at providing an estimation of fragility function parameters based on the maximization of the likelihood function, L, assuming a log-normal cumulative distribution function to define the probability that a ground

motion with $IM = x$ will cause the block to collapse (uplift):

$$P_{RO(UP)}(EDP \geq C|IM = x) = \Phi\left(\frac{\ln(x/\mu)}{\beta}\right) \tag{16}$$

where μ is the median of the fragility function and β is the logarithmic standard deviation of IM. These can be computed after maximization of the likelihood function. Equation (16) differs from Equation (15) from the nature of the data used to compute the CDF, which are in terms of IM here, whereas P_{ex} are function of EDP.

Similarly, it is possible to create bivariate FC in the three dimensional space $P_{f,C}$ - IM_1 - IM_2,[18] assuming a bivariate exponential correlation between IM_s and the structural demand.

4.4 | Seismic demand hazard model

Comparing it to the previous procedure, the seismic demand hazard model is a more robust metric unconditional to the given IM. Indeed, this model also considers the likelihood that a certain LS will be exceeded over the life of the structure, starting from the ground motion hazard curve. The output of the methodology is the seismic demand hazard, λ_{EDP}, that provides the exceedance rate of a specific LS in terms of EDP, and can be computed with the following:

$$\lambda_{EDP}(edp) = \int_0^\infty P_{EDP|IM}(edp|im)\left|\frac{\mathrm{d}\lambda_{IM}(im)}{\mathrm{d}IM}\right|\mathrm{d}IM \tag{17}$$

The whole process, suggested by Bradley[19] is updated here to properly consider non-rocking and overturning events, and can be summarized in the following steps: (i) definition of ground motion hazard (commonly available from standards in terms of PGA, see Figure 2a); (ii) seismic response analysis for several ground motions, scaled at multiple intensity levels previously defined by the ground motion hazard, that is multiple stripes analysis (MSA); (iii) computation of the distribution of each set of SR results for each IM level; (iv) maximization of the likelihood functions for NR and RO observations; (v) integration within the derivative of the seismic hazard curve, λ_{IM} to finally obtain the seismic demand hazard, λ_{EDP}. Being the ground motion hazard discretely defined only for m intensity measure levels (such as 9 PGA values for $30 < RP < 2475$ (Figure 2a)), Equation 17 simply becomes the sum over the m stripes of the product between the i^{-th} probability of exceeding the k^{-th} LS, $P(EDP \geq edp_k|IM = im_i)$, and the i^{-th} seismic hazard difference, $\Delta\lambda_i$:

$$\lambda_{EDP}(edp_k) = \sum_{i=1}^{m} P(EDP > edp_k|IM = im_i)|\Delta\lambda_i| \tag{18}$$

Because of this discretization, two extreme values of the ground motion hazard curve are lost during the numerical derivative computation, thus only internal values of intensity levels can be devoted for the NLTH analyses. Nevertheless, one additional point can be appended on the seismic ground motion hazard curve of Table 4, assuming a logarithmic linearization around the reference RP, as suggested by Bradley.[19]

The full process is graphically represented in Figure 4 for the extrapolated data from reference sample analysis. The amplified site-related hazard curve is shown in Figure 4a. The probability of exeedance is computed as the complementary cumulative lognormal-type distribution obtained for each group of SR responses $P_{k,i} = 1 - cdf(edp_k|im_i)$ (Figure 4b,d). These are combined with corresponding probabilities of overturning and uplift, P_{RO} and P_{UP} according to Equation 14 (see Figure 4f). The seismic demand hazard curve (Figure 4c) is finally constructed with the sum over the m levels of the product between each $P_{k,i}$ and the corresponding $\Delta\lambda_i$ leading to evaluating the annual exceedance rate in function of a given EDP . The lognormal probability density function, pdf(edp) is also shown in Figure 4d , while the likelihood function for RO cases is shown in Figure 4e.

It is worth noting that the probability of exceeding a given limit state $P_{k,i}$, is equivalent to the conditional probability P_{ex} already defined in Equation 15 necessary to draw FC. However, in this approach, mean and standard deviation are directly obtained by the hypothesis of lognormal distribution of ith group of SR response data, while fragility analysis is developed assuming median demand after linear regression analysis of the logarithms (Section 4.3).
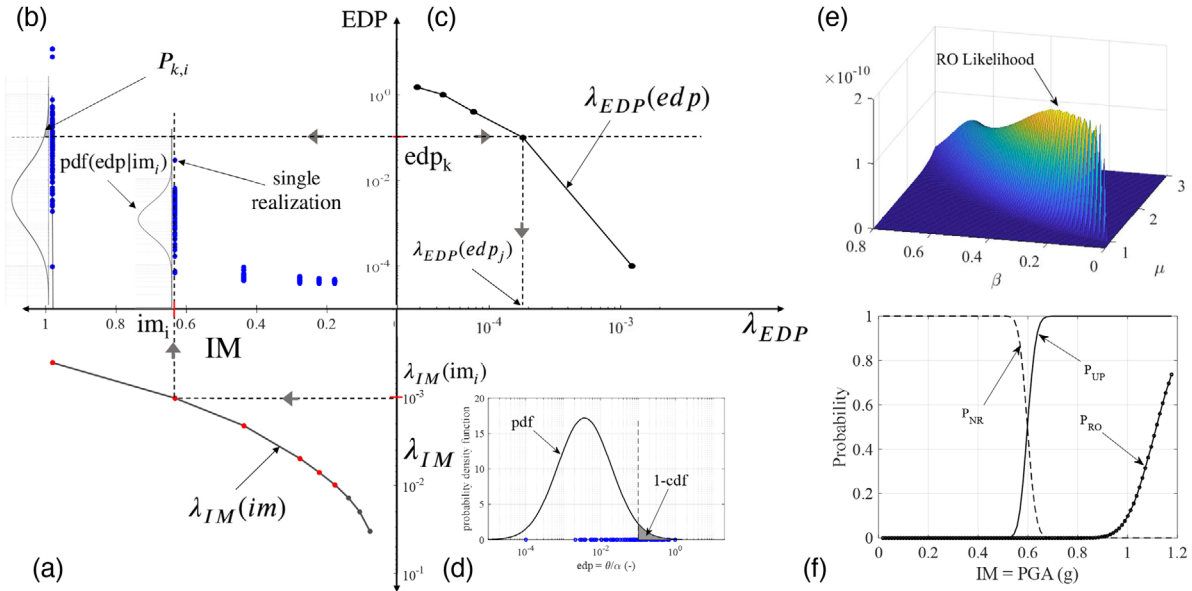
FIGURE 4 Seismic demand hazard analysis process: (a) amplified ground motion hazard curve (selected IM levels in red dots); (b) lognormal distributions of results data; (c) seismic demand hazard curve (SDHC); (d) lognormal probability density function for one set of NLTH analyses; (e) RO Likelihood function; (f) "categorical" probabilities
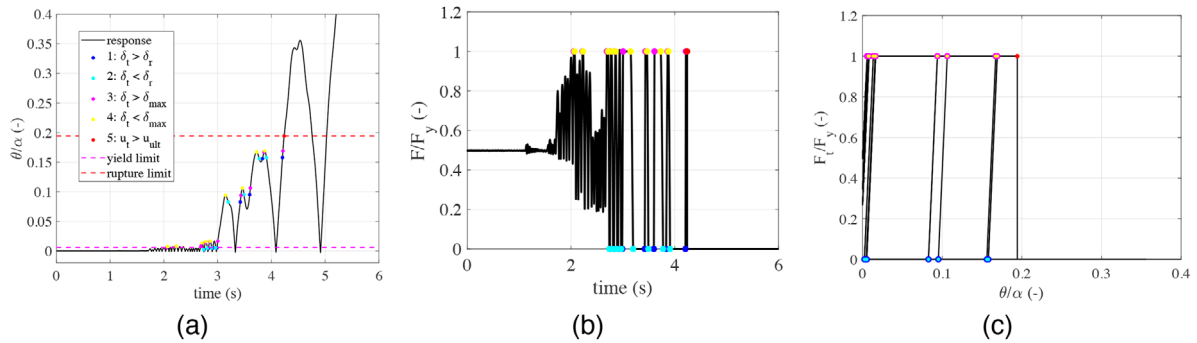

FIGURE 5 Results of a single realization related to $H/s = 10$, $s = 0.60$m, $\epsilon_u = 2\%$, $f_y = 235$ MPa and +20120429_MIR02, record: (a) normalized rotation time-history; (b) normalized tie-rod force time-history; (c) normalized tie-rod hysteresis

5 | RESULTS AND DISCUSSION

The time-history response of one-sided restrained masonry wall in terms of normalized rotation and normalized tie force are shown in Figure 5 for a single simulation (record: +20120429_MIR02 $\epsilon_u = 2$ %), together with the normalized tie force hysteresis. These graphs are useful to correctly interpret the seismic behavior of each case, also evaluating possible anomalies in the response. Each phase transition is depicted with a colored circle according to different phases defined in the constitutive law (Section 2 and Figure 1c).

5.1 | IM performance

The fragility model effectiveness relies upon the IM performance, since its assumption conditions the uncertainties of the computed fragility curves. The best IM can be selected according to different criteria and parameters. The *efficiency* can be evaluated through $\beta_{D|IM}$[25] related to the variation of the estimated demand for a given IM, thus a lower value of $\beta_{D|IM}$ implies a more efficient IM; commonly, the coefficient of determination, $R^2 = 1 - [\sum(\ln D - \ln S_D)^2]/[\sum(\ln D - \overline{\ln D})^2]$ is used to evaluate the dispersion of data, too. The regression parameter, b, the slope of the estimated demand, is a measure

TABLE 6 IM correlation coefficients for masonry walls in one-sided motion and in free or restrained configuration

Unrestrained sample									
Univariate					**Bivariate**				
IM	**b**	**$\beta_{D\|IM}$**	**ζ**	**R^2**	**IM_1**	**IM_2**	**$\beta_{D\|IM}$**	**R^2**	**ρ**
I_a	1.119	**0.988**	0.883	**0.574**	SI_H	I_a	**0.926**	**0.626**	0.743
RMSA	**1.863**	1.125	**0.604**	0.447	PGV	I_a	0.929	0.623	0.827
CAV	1.460	1.131	0.774	0.442	I_a	L_m	0.934	0.619	0.631
PGV	1.374	1.157	0.842	0.416	PGV	RMSA	0.986	0.576	0.744
IF	1.194	1.188	0.995	0.384	PGV	I_F	1.154	0.419	**0.987**
Restrained reference sample									
Univariate					**Bivariate**				
PGA	**6.952**	**1.332**	**0.192**	**0.570**	**PGA**	I_a	**1.194**	**0.654**	**0.866**
I_a	1.648	1.587	0.963	0.389	PGA	CAV	1.221	0.638	0.642
RMSA	3.378	1.658	0.491	0.333	PGA	I_F	1.265	0.612	0.559
CAV	1.210	1.837	1.518	0.182	PGV	RMSA	1.654	0.336	0.744
PGV	0.946	1.891	1.998	0.133	PGV	I_F	1.886	0.137	**0.987**

Note: In bold the most practical, efficient and proficient IM.

of *practicality*, that is, a lower value of b implies a less practical IM; finally, $\zeta = \beta_{D|IM}/b$ quantifies the *proficiency*, that is an indication of the uncertainty introduced into the analysis by the use of a particular IM.[33] The IM performance for bivariate FC can simply be computed with dispersion parameters R^2 or $\beta_{D|IM}$ as the calculus of b and ζ can be misleading. Moreover, an estimation of the quality of correlation between two IM (x = value depending on IM_1, y = value depending on IM_2) can be given by the Pearson's linear correlation coefficient,

$$\rho = \frac{\sum_i \left(x_i - \overline{x}\right)\left(y_i - \overline{y}\right)}{\sqrt{\sum_i \left(x_i - \overline{x}\right)^2 \sum_i \left(y_i - \overline{y}\right)^2}} \tag{19}$$

Dimitrakopoulos and Paraskeva[25] stated that the best IM for univariate FC for free-standing rocking structures under near-fault excitations are PGA and PGV, which are also conventional earthquake parameters, while the pair PGA and PGV/PGA forms a powerful combination for a reliable prediction through bivariate FC.

The fragility analysis is performed firstly considering the analytical coefficient of restitution (COR) (Housner[6]) and then taking into account the experimental value of one-sided rocking according to Sorrentino et al.[8]. In case of analytical COR, the sensitivity analysis reveals that poor correlation coefficients are found for any IM, being $R^2 < 0.6$. The correlation is even poorer for restrained walls (Table 1), if compared to those unrestrained, thus it is hard to select an optimal IM. Among the IM considered for restrained walls, PGA ranks the first in terms of practicality, efficiency and proficiency, followed by Arias intensity I_a, root mean square acceleration RMSA, cumulative absolute velocity CAV, and peak ground velocity PGV (Table 6) if sorted by R^2, whereas in case of unrestrained block samples (i.e., absence of tie-rod) the most efficient IM is I_a and the most practical and proficient is RMSA (Table 6). As visible in Table 6, acceleration-related IM prevail to the velocity-related IM for both unrestrained and restrained blocks. Similar values are obtained for the bivariate correlation analysis. A bi-planar regression performed for bivariate FC also reveals a differentiated response if one compares restrained to unrestrained samples. Indeed, the most efficient (less dispersion) IM couple for the restrained geometry are PGA and I_a, whereas for unrestrained blocks one has Housner intensity SI_H and I_a (Table 6), confirming the superiority of acceleration-based IM over velocity-based IM. However, if one considers their correlation through the Pearson's correlation coefficient, the best couple results to be PGV and I_F for both unrestrained and restrained reference sample. Apparently, there is a negligible increase in performance of bivariate FC over univariate FC as both share similar dispersion parameters $\beta_{D|IM}$.

It is important to point out that optimal IM are here selected through correlation analysis between dynamic analyses response data and IM values that are calculated from scaled waveforms (according to the PGA values of the seismic hazard curve). The amplitude scaling is a conventionally accepted procedure by the research community.[34] Moreover, the linear regression analysis is only performed over SR data, possibly neglecting many responses and leading to not-sufficiently

reliable results. This issue is highlighted in cases of IM = PGA for restrained samples, where only for PGA ≥ 0.63 g the blocks uplifts, thus neglecting four entire set of PGA levels.

Additional analyses are also performed for unrestrained wall in order to study the influence of a different COR. A more realistic value is assumed to consider the one-sided rocking.[8] In particular, two different values of COR are assumed depending on the direction of rotation[8]:

$$e_{exp,inward} = -1.05 \cdot e_{an,2s} \cdot e_{an,tr} = -1.05 \left(1 - \frac{2}{3} \sin^2 \alpha\right) \left(1 - \frac{3}{2} \cos^2 \alpha\right),$$ (20)

where $e_{exp,inward}$ is assumed for the inward rotations and accounts for energy dissipated through the impact with base corners and transversal walls. The coefficient of 1.05 has been used as experimental correction recommended in Sorrentino et al.[8] valid if damping remains constant with amplitude and if the whole time-history is considered. The results are displayed in Figure 7 and discussed later.

Whereas, for outward rotations it is assumed as the following:

$$e_{exp,outward} = 0.95 \cdot e_H$$ (21)

The results for this latter case show that the IM are better correlated. They are not reported for the sake of brevity but briefly discussed in the following. Both PGA and I_a show higher value of R^2 (up to 0.664) and $\beta_{D|IM}$. These aspects further justify the assumption of the analytical restitution coefficient. However, PGV ranks second when the experimental restitution coefficient is assumed, while it was in the forth position in the previous case. Moreover, PGV has the third best practicality, coherently with the previous case. The RMSA, which was second in the previous case, has the lower ζ (best proficiency) and is the second most practical. Analogously, bivariate IM are better correlated having higher values of R^2 with respect to the analytical coefficient of restitution. The best correlated couples are PGA and PGV, followed by PGA and PGV/PGA both having the same value of $R^2 = 0.803$.

Fragility analysis for both univariate (I_a) and bivariate (PGV and RMSA) FC is shown in Figure 6 in case of unrestrained and restrained reference geometry. Fragility curves obtained for the restrained reference wall clearly show a flatter trend and a lower probability of exceedance for both uni- and bi-variate cases (Figures 6f,k) if compared to the unrestrained wall. As expected, the presence of elasto-plastic tie rods highly mitigates the seismic vulnerability of rocking blocks, effect remarkable for LS_i, with $i \geq 1$.

A straightforward graph to assess the effectiveness of the ties is given by the reduction percentage of conditional probability expressed as $\Delta P_{f,C} = (P_{f,C,restr} - P_{f,C,unrestr}) \times 100$ (as defined in Equation 14). From such a graph, it is possible to state the earthquake intensity level for which the anti-seismic device is more effective. For instance, for LS_4 the maximum reduction of $P_{f,C}$ is obtained for high intensity earthquakes whereas for LS_0 for low-intensity shocks (Figure 6i). Similarly, Figure 6l shows the reduction percentage's trand of $P_{f,C}$ in case of multivariate FC.

The influence of different coefficient of restitution is shown in Figure 7 in terms of regression analysis and probability of exceedance for IM = I_a. As previously anticipated, the IM is better correlated and results in a lower estimation of EDP, leading to flatter probability of exceedance (P_{ex} is about 30% less for I_a = 1000 cm/s). Such a result further justify the assumption of conservative results when using the analytical coefficient of restitution.

5.2 | Influence of the number of seismic inputs on SDHC

The reliability of probabilistic models (Sections 4.3 and 4.4) strictly depends upon the number of considered seismic inputs. When the number of analyses performed for each IM level is doubled from 24 to 48 (leading to a total of $6 \times 48 = 288$ analyses for each sample), and then from 48 to 96, the seismic demand hazard curve (SDHC) undergoes noticeable changes (Figure 8), especially for higher values of normalized rotations. This is valid for both unrestrained block and reference geometry (Table 1). The relatively small difference obtained for $\theta/\alpha = 10^{-4}$, and reference geometry (Figure 8(b)) can be due to the high variability of results around non-rocking responses. Given the importance of accounting for a sufficient number of data for reliable results, it is decided to perform 96 analyses for each IM level. Indeed, the difference between SDHC computed with 48 or 96 IM levels appears negligible. Such a sensitivity analysis is recommended as simple but effective tool to state the minimum number of IM levels to consider to qualify the computational process as reliable.
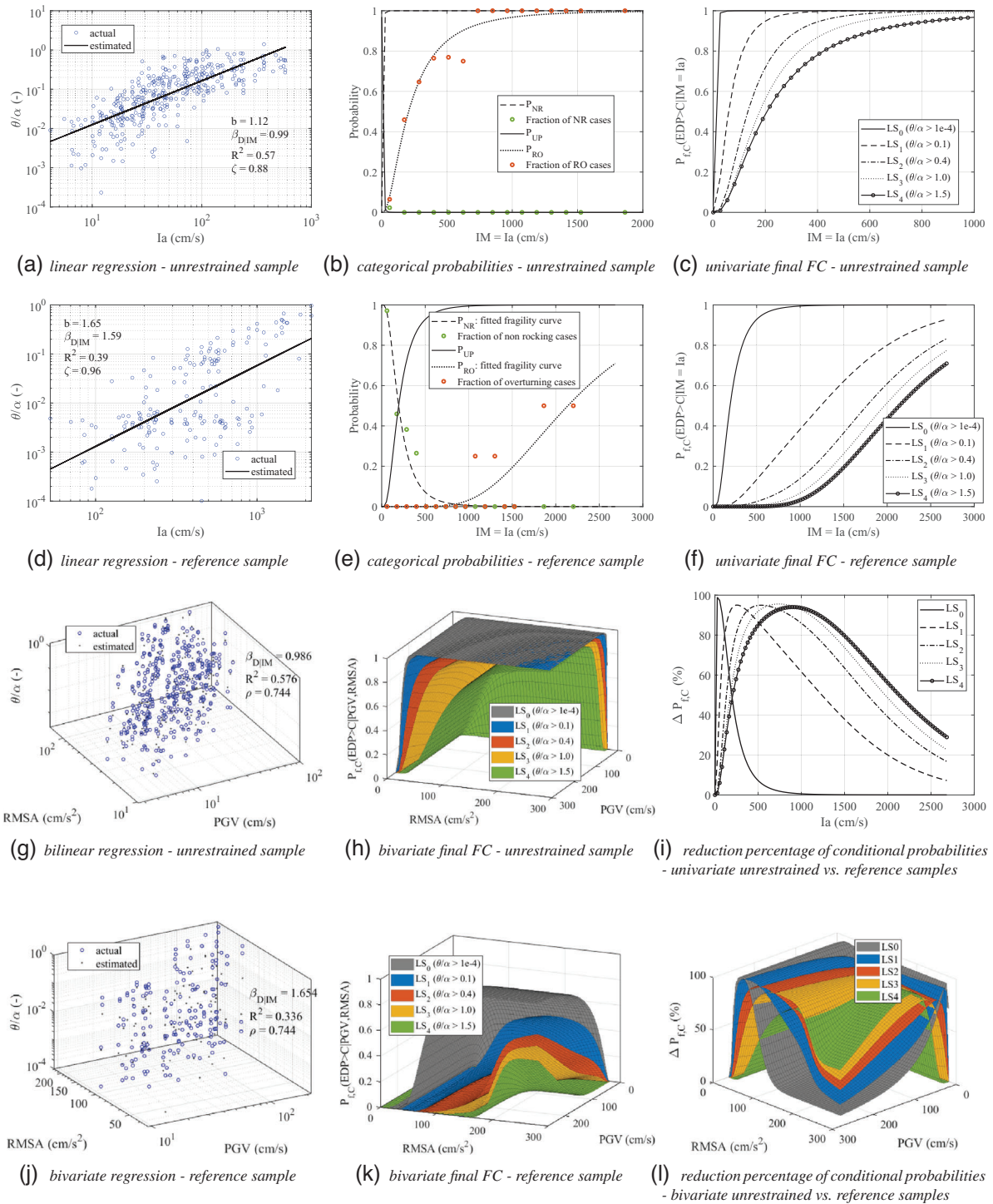
(a) *linear regression - unrestrained sample*

(b) *categorical probabilities - unrestrained sample*

(c) *univariate final FC - unrestrained sample*

(d) *linear regression - reference sample*

(e) *categorical probabilities - reference sample*

(f) *univariate final FC - reference sample*

(g) *bilinear regression - unrestrained sample*

(h) *bivariate final FC - unrestrained sample*

(i) *reduction percentage of conditional probabilities - univariate unrestrained vs. reference samples*

(j) *bivariate regression - reference sample*

(k) *bivariate final FC - reference sample*

(l) *reduction percentage of conditional probabilities - bivariate unrestrained vs. reference samples*

FIGURE 6 Univariate (IM = I_a) and bivariate (IM$_1$ = PGV and IM$_2$ = RMSA) fragility analyses: (a), (b), (c), (g) and (h) unrestrained sample; (d), (e), (f), (j) and (k) reference sample; (i) and (l) reduction percentage of conditional probabilities: unrestrained versus restrained reference samples

5.3 | Influence of the geometry

Literature studies about unrestrained rocking blocks demonstrate that, among blocks with the same aspect ratio, stockier blocks are more stable, while blocks with smaller size (smaller thickness) are more vulnerable to earthquake-type actions.[35] AlShawa et al.[17] also confirmed this statement for restrained walls: they showed that the influence of
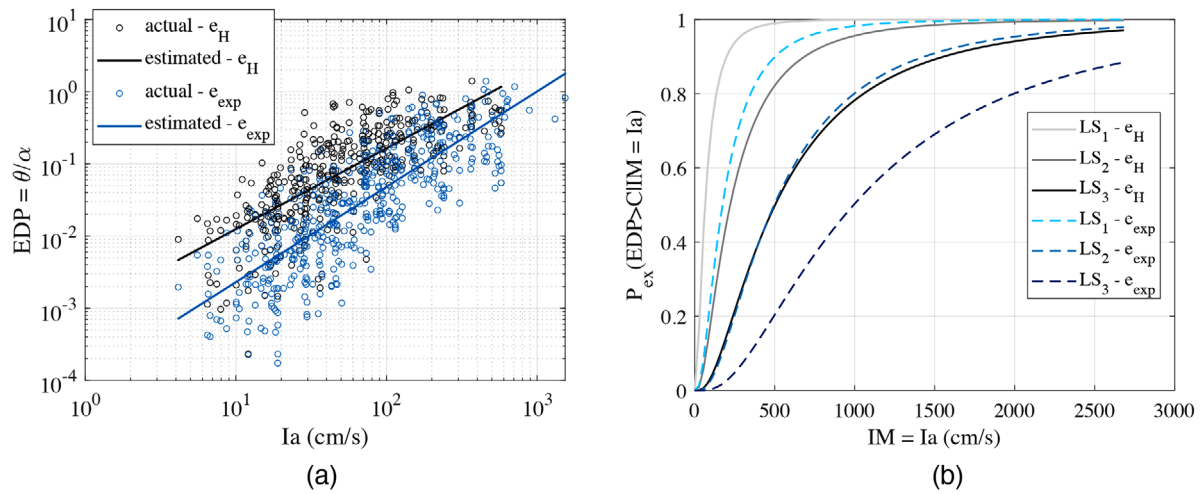
FIGURE 7 Influence of coefficient of restitution for univariate (IM = I_a) for unrestrained sample: (a) linear regression; (b) probability of exceeding LS1, LS2 and LS3
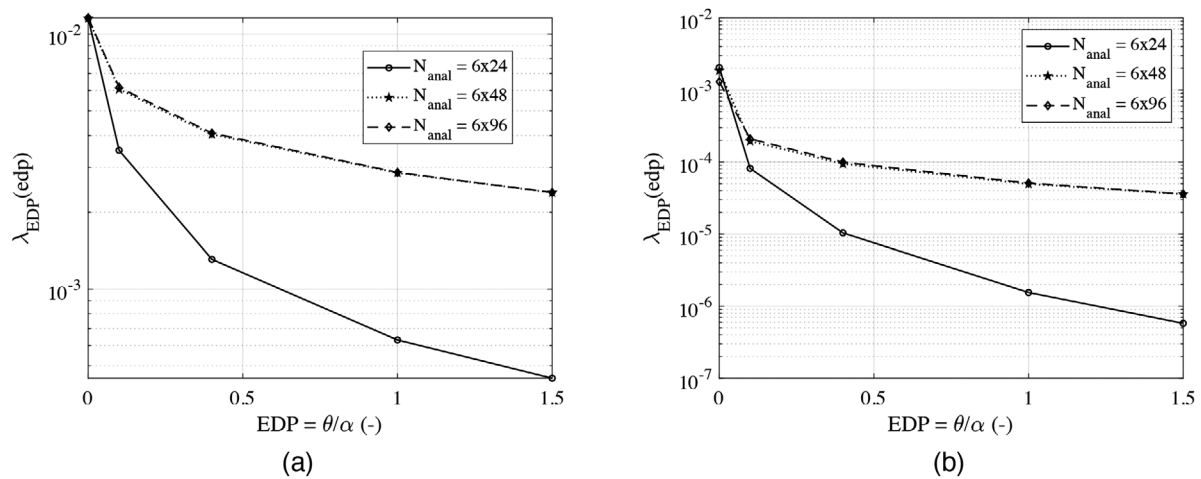
FIGURE 8 Variation of SDHC by changing the number of IM levels assumed in the probabilistic analysis: (a) unrestrained sample; (b) restrained reference sample with EP tie

the aspect ratio is negligible, whereas blocks with different size tend to behave differently (i.e., blocks with smaller thickness are more vulnerable from a seismic point of view). In order to better understand the influence of slenderness and to study the scale effect, three different aspect ratios ($H/s = [8, 10, 12]$, $s = 0.6$ m) and three thickness values ($s = [0.30, 0.60, 0.90]$ m, $H/s = 10$) are considered, totally defining five geometries (Table 2). The negligible influence of slenderness in case of restrained blocks is confirmed here in terms of FC (Figure 9d) and SDHC (Figure 9e). In Figure 9d, the only FC for limit states $LS_1 \leq LS \leq LS_3$ are shown for the sake of readability; they are flatter and demonstrate a very low influence of the aspect ratio (Figure 9a-c). Recalling that λ_{EDP} provides the annual exceedance rate of a specific LS, the maximum difference is obtained when passing from H/s = 8 (equal to that of H/s = 10) ($\lambda_{EDP} \simeq 1/35,000$) to H/s = 12 ($\lambda_{EDP} \simeq 1/30,000$), for LS_4. Although the difference in terms of return period is about 5000 years, one has a negligible difference in terms of probability, which has absolute values of about 3^{-5}, thus very low.

If the aspect ratio is fixed to $H/s = 10$, the scale effect can be studied by changing the block size, for instance by varying the thickness s (Figure 10). In this case, both FC and SDHC are affected by the difference of thickness: in particular, for LS_1, LS_2, and LS_3 the FC exhibit a monotonic trend (Figure 10d): indeed, the smaller walls have higher probability of exceedance, for a given IM = PGA. This is evident for high intensity earthquakes (PGA $\geq$ 0.9 g). It is interesting to note that the size of the block also influences the response in terms of SDHC as shown in Figure 10e. Here, although the bigger wall has an intermediate behavior for LS_0, a monotonic trend is again observed for the remaining LS (i.e., lower
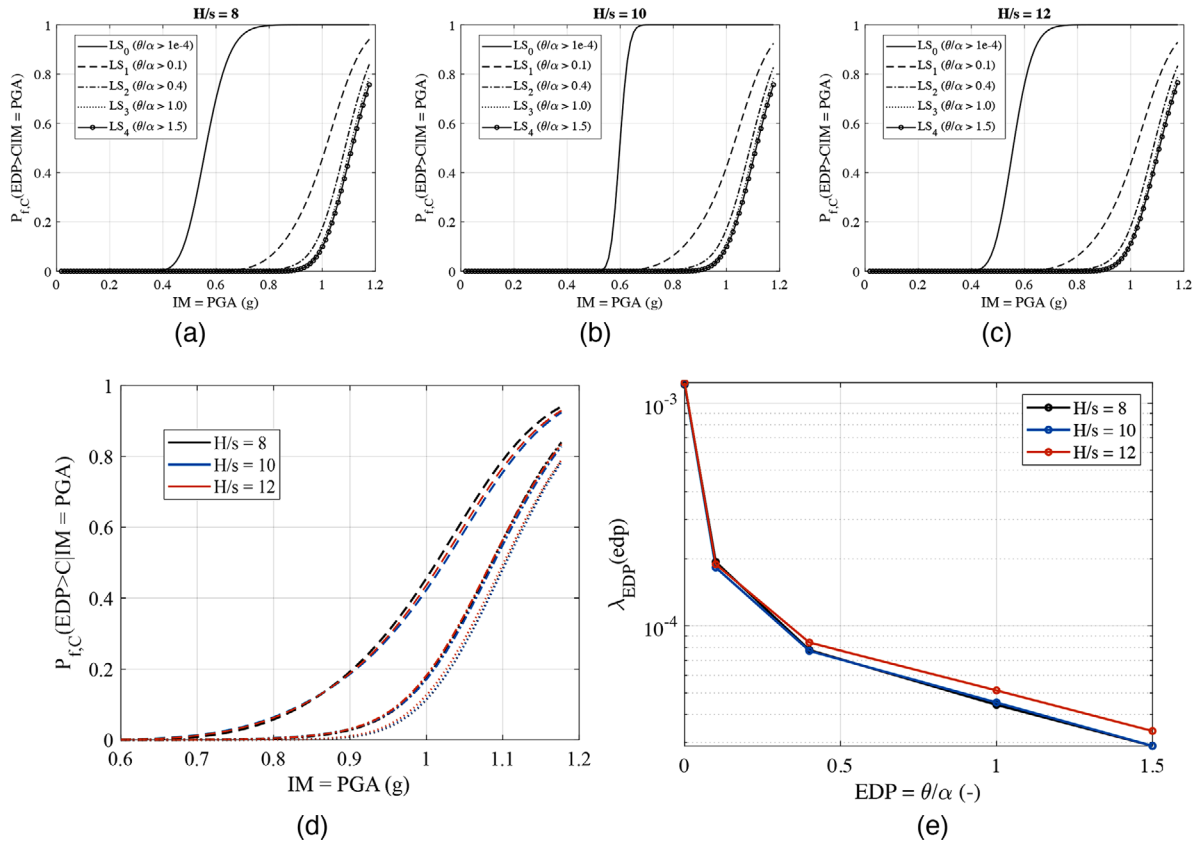
FIGURE 9 Influence of aspect ratio H/s in terms of (a-c) FC for all LS; (d) FC for $LS_{1,2,3}$ for PGA > 0.6 g (dashed lines: LS_1; dashed-dotted lines: LS_2; dotted lines: LS_3) and (e) SDHC

exceedance rate for higher size). The differences observed for the FC are flattened out for the SDHC, for which the hazard parameter comes into play. Therefore, in a seismic vulnerability assessment it is necessary to preliminarily analyze the FC which could reveal behaviors worth of further investigations. In other words, to read solely SDHC could be limiting to study the scale effect.

5.4 | Influence of the ductility

Despite the well known ductile properties of modern steel, it is a matter of fact that historic tie-rods, frequently found in seismically vulnerable masonry buildings, may be characterized by rather brittle behavior, with quite low values of ultimate strain $\epsilon_u \ll 10\%$.[15] The influence of tie-rod ductility is studied herein considering five values of ultimate deformation, $0 < \epsilon_u < 20\%$ (Table 2). The whole set of simulations is shown in Figure 11a, and the beneficial aspect of increasing ductility (from $\epsilon_u = 2\%$ to 10%) is demonstrated for the same geometry in Figure 11b. When a more ductile tie is adopted, this is able to re-center the block stabilizing the response, whereas a weaker tie-rod undergoes failure increasing the oscillation amplitude up to collapse and wall overturning. The influence of ductility is also studied in terms of FC, which are shown here for all limit states in Figure 12. From the analysis of the results condensed in Figure 13a, it can be stated that a brittle behavior of the tie-rod strongly increases the seismic risk, passing for instance from a probability of exceeding a limited rocking limit state of 30% (brittle tie-rod) to 8% (low-ductility or $\epsilon_u = 2\%$) for a given $PGA = 0.8g$. This aspect demonstrates the extremely beneficial effect of ensuring an even low ductility of the tie-rod to remarkably reduce the seismic risk of the out-of-plane mode. The beneficial effect of assuming medium and high ductility values emerges when ultimate rocking LS are considered, as their behavior differs for higher normalized rotations of the wall.

From the comparison of the results in terms of λ_{EDP} (Figure 13b), it is self-evident that restrained walls are characterized by a safer response, if compared to unrestrained blocks. Moreover, there is a clear divergence between the SDHC of brittle (blue curve) and ductile tie-rod, especially for increasing EDP values. Up to a limited rocking LS ($\theta/\alpha = 0.4$), there is
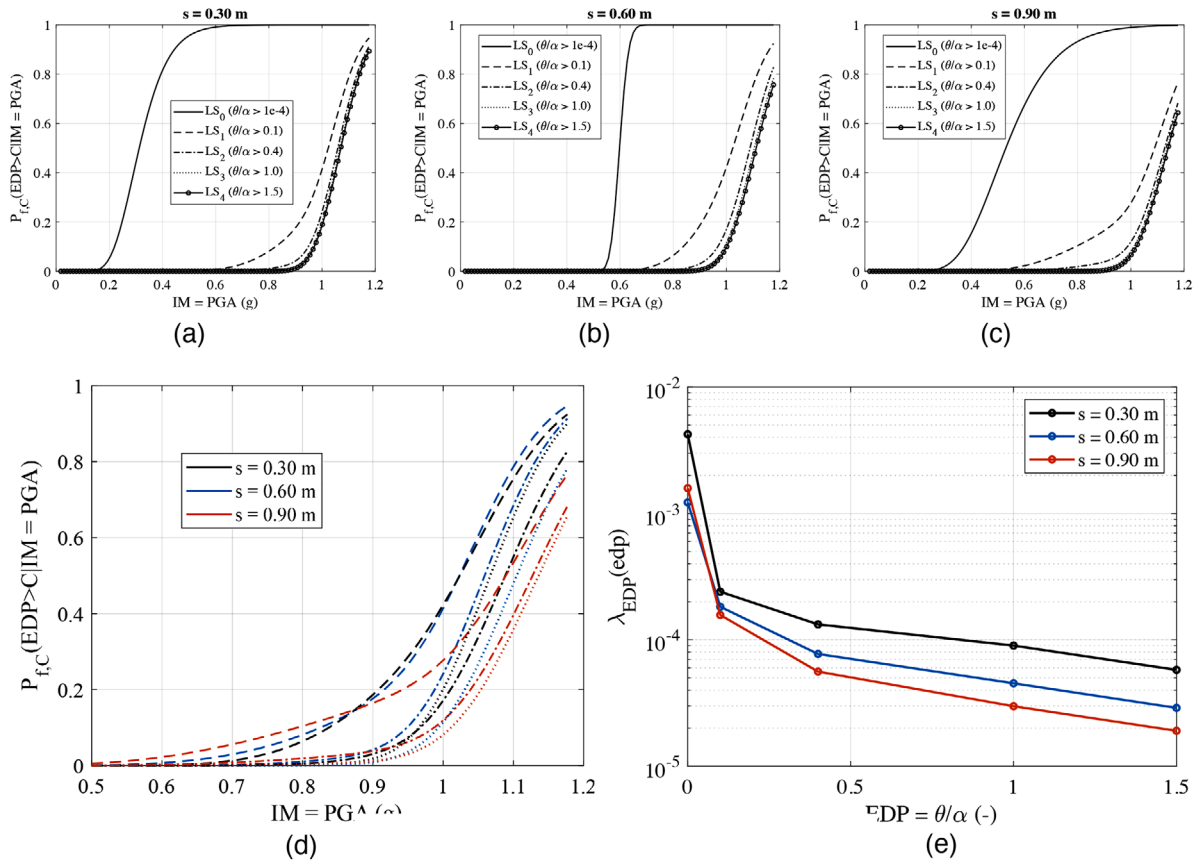
FIGURE 10 Influence of size with variable block thickness s, for restrained block with a reference slenderness, $H/s = 10$ in terms of (a-c) FC for all LS; (d) FC for $LS_{1,2,3}$ (dashed lines: LS_1; dashed-dotted lines: LS_2; dotted lines: LS_3) and (e) SDHC
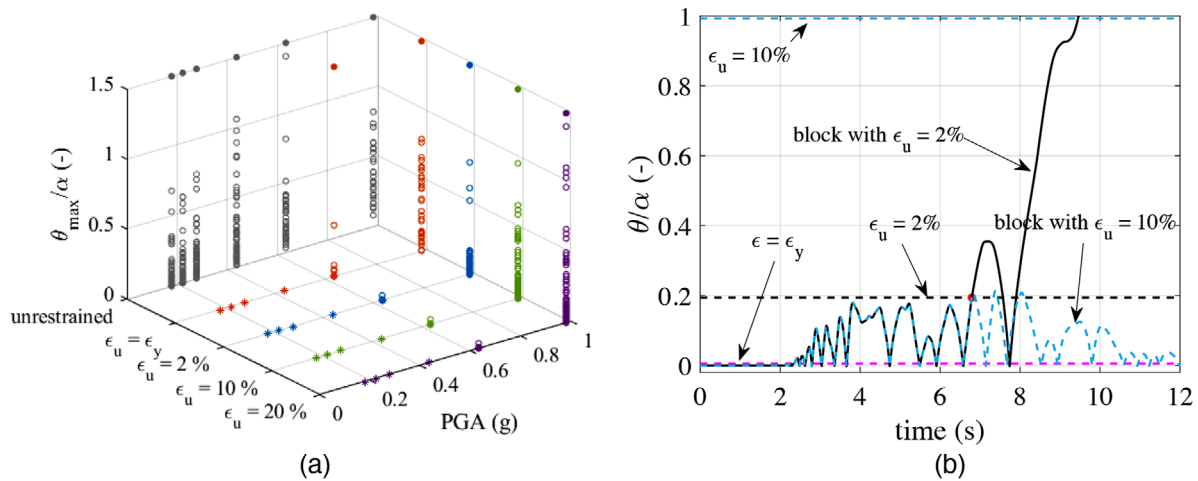

FIGURE 11 Influence of ductility in terms of (a) total results (stars for NR cases; empty circles for SR cases; full circles for RO cases); (b) normalized rotations time-histories for two simulation under Norcia 2016/08/24 ID 4, Table 5

not substantial difference between the curves associated to a tie-rod of whatever ductility. Moreover, the probability of exceeding LS_2 is very low ($\simeq 1/7000$) for low ductile tie. This aspect again confirms that an excessive ductility is useless in terms of reduction of seismic risk, unless very high rotational demands are considered or very low annual exceedance rate is requested.
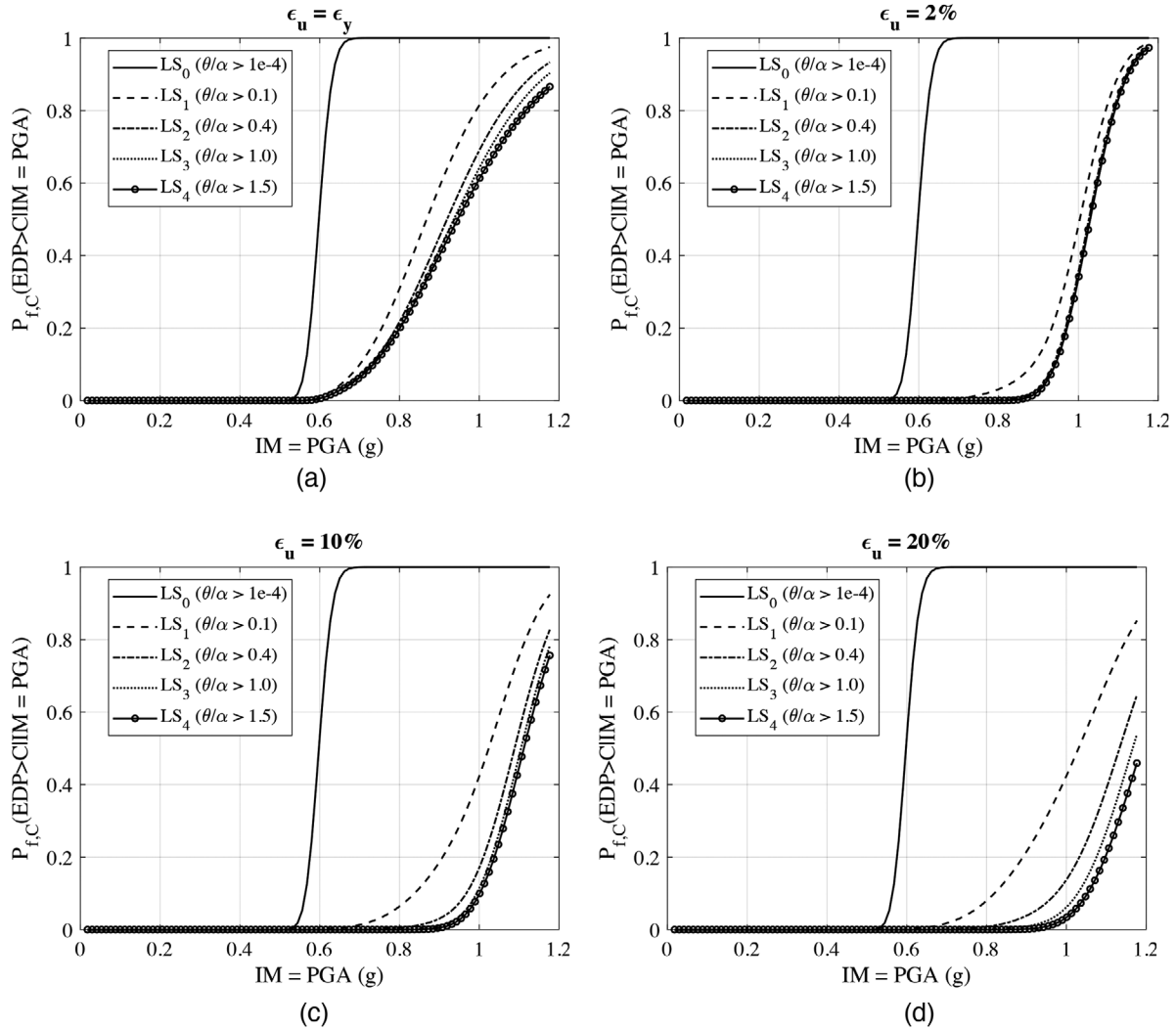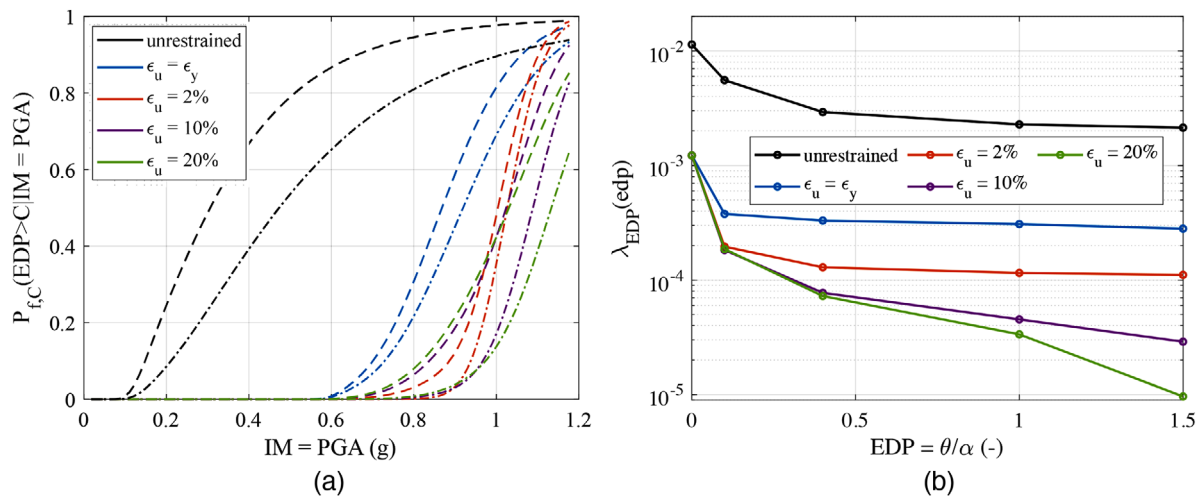
FIGURE 12 Influence of ductility changing ϵ_u values

FIGURE 13 Influence of ductility changing ϵ_u values in terms of: (a) FC for $LS_{1,2}$ (dashed lines: LS_1; dashed-dotted lines: LS_2) and (b) SDHC
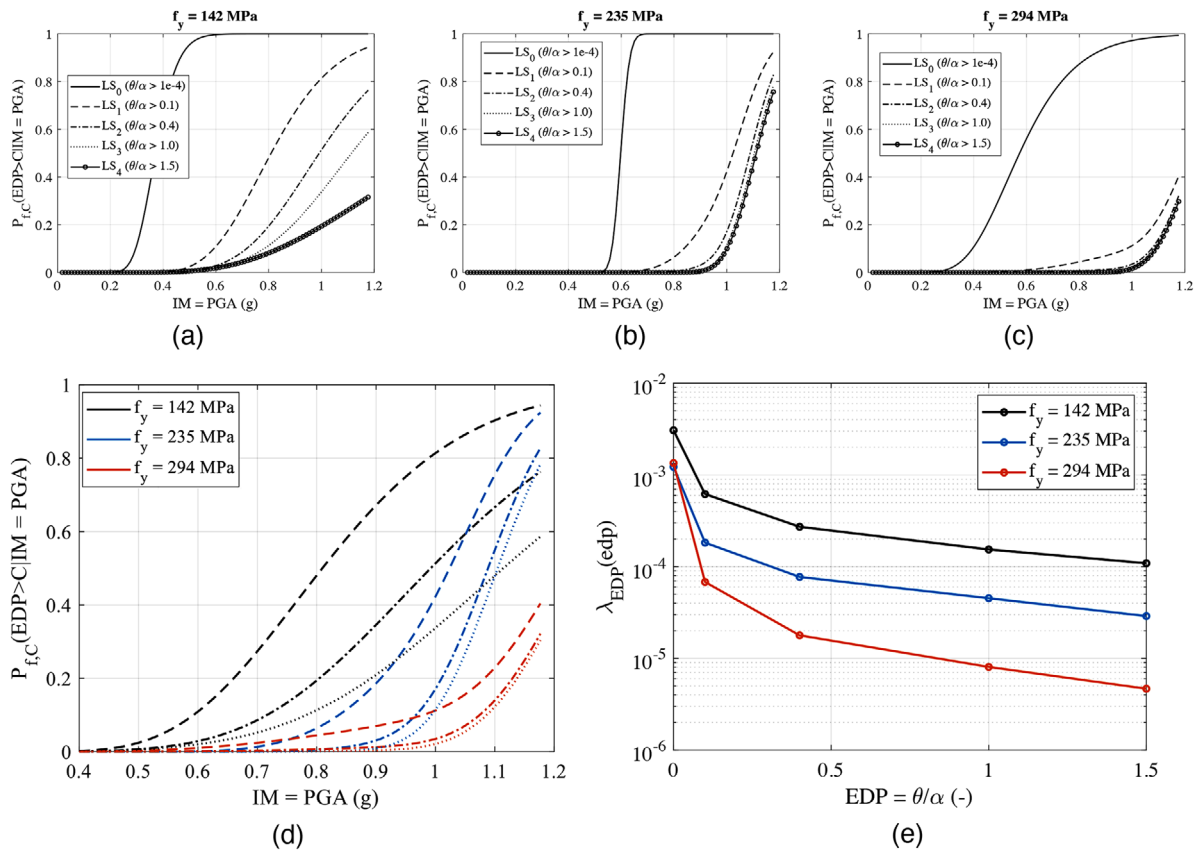
FIGURE 14 Influence of tie-rod axial strength, f_y: (a-c) Fc for all LS; (d) FC (LS$_{1,2,3}$); (e) SDH curves

5.5 | Influence of tie axial strength

This paragraph discusses the influence of the tie-rod strength on the seismic vulnerability of the walls under the set of the selected 96 earthquakes. Looking at Figure 14e, it is evident the strong influence of this parameter in the probabilistic response. Among the three strength values considered, low (142 MPa), medium (235 MPa) and high (294 MPa) resistance, those medium and high do not exhibit any variation of annual exceedance rate for what concerns the uplift state. That is to say that for a serviceability limit state, modern tie-rods (which have at least 235 MPa of strength) are not required to have particularly high strength to avoid the exceedance of the uplift limit state (Figure 14). By contrast, considering ultimate limit states, the gap is definitely increasing: for instance, for a near-collapse limit state the annual exceedance rate is 1/200,000 for a high strength tie-rod and 1/9000 for a low strength tie-rod. This parameter is therefore much more influencing the seismic risk of restrained walls rocking out-of-plane.

6 | CONCLUSIONS

This paper analyzed the seismic behavior of unrestrained and restrained masonry walls in one-sided motion with probabilistic methods. The horizontal restraints considered for the out-of-plane response of masonry walls were elasto-plastic tie-rods with variable diameter, strength and ductility. A parametric analysis was performed with a specifically developed MATLAB code, selecting walls with five typical geometries, five ultimate strains and three strength values for the steel tie-rods under 96 seismic records scaled to 6 intensity measures (IM) levels. Two probabilistic models were employed, one for obtaining univariate and bivariate fragility curves (FC), and the second one for computing the seismic demand hazard curves (SDHC), capable of correlating the hazard site to the seismic vulnerability assessment of out-of-plane modes, separately computing the probability of overturning (categorical probability) and the probability of exceeding four specific limit states. The following outcomes can be drawn from the analysis:

- Fragility analysis effectiveness is quite low for restrained rocking blocks as no IM performed well. Indeed R^2 values are less then 0.6 for univariate correlation, and less then 0.65 for bivariate correlation. This is probably because regression analysis is solely based upon safe rocking cases, and seismic inputs are scaled for discrete PGA levels. Thus, correlation coefficients may be misleading in cases of too large PGA intervals, possibly requiring additional analyses with more dense PGA intervals. Unfortunately, available site-related seismic hazard curves only offers discrete PGA intervals to be used. Moreover, restrained samples behave quite stable with uplift cases only for PGA ≥ 0.62 g, yet reducing data for correlation analysis.

- Although the correlation coefficients are not so relevantly high, the acceleration based IM seems better correlated, both for restrained and unrestrained walls. More in detail, the peak ground acceleration PGA performed well in terms of practicality, efficiency and proficiency, followed by Arias intensity I_a in terms of efficiency for restrained walls, and root mean square acceleration RMSA (practical and proficient) for unrestrained walls. As for the bilinear regression, IM pair performance is also quite low. The IM pair PGA and I_a shows well correlation for restrained walls, while Housner intensity SI_H and I_a for those unrestrained. Nevertheless, when considering the correlation through the Pearson's coefficient, the velocity based IM (Fajfar index IF, and peak ground velocity PGV) show better performance for both boundary conditions;

  Additional analyses carried out for the unrestrained case using experimental (more realistic) coefficient of restitution showed better performance of IM with respect to those with analytical value of coefficient of restitution. Results are coherent and less conservative but further analyses are necessary for studying the energy dissipation in one-sided rocking walls.

- The number of considered seismic input, and consequently the number of analyses carried out, has a great impact on the SDHC, therefore it is recommended, as commonly made for finite element models, to increase its number up to negligible differences in SDHC; through this novel procedure, 96 analysis are sufficient to reach stable results;

- The slenderness variation (height to thickness ratio = 8-10-12) does not play a significant role either in the change of FC neither in that of SDHC for restrained rocking walls;

- By contrast, the variation of block size (thickness) influences more the FC rather than the SDHC for restrained walls. In particular, the typical scale effect (between two blocks of same slenderness, the bigger is less seismically vulnerable) is mainly observed for limited and moderate rocking limit states;

- A brittle behavior of the tie-rod strongly increases the seismic risk, passing for instance from a probability of exceeding a limited rocking limit state of 30% (brittle tie-rod) to 8% (low-ductility tie-rod) for a given PGA = 0.8 g. This aspect demonstrates the extremely beneficial effect of ensuring an even low ductility of the tie-rod to remarkably reduce the seismic risk of the out-of-plane mode. However, an excessive ductility ($\epsilon_u \geq 10\%$) is useless in terms of reduction of seismic risk, unless very high rotational demands are considered ($\theta/\alpha \geq 0.4$) or very low annual exceedance rate ($\lambda_{EDP} \leq 1/10,000$) is requested.

- For the limited, moderate and ultimate rocking limit states, the tie axial strength influence is not negligible. This parameter has a great impact on the annual exceedance rate passing from a high strength to a low strength (typical of historic tie-rods found in existing masonry buildings) of the tie-rod.

CONFLICT OF INTEREST
The authors declare no potential conflict of interests.

DATA AVAILABILITY STATEMENT
The data that support the findings of this study are available from the corresponding author upon reasonable request.

ORCID
Fabio Solarino https://orcid.org/0000-0001-5030-0982
Linda Giresini https://orcid.org/0000-0001-6913-7468

REFERENCES

1. Griffith MC, Magenes G, Melis G, Picchi L. Evaluation of out-of-plane stability of unreinforced masonry walls subjected to seismic excitation. *J Earthquake Eng*. 2003;7:141–169. https://doi.org/10.1080/13632460309350476
2. DeJong MJ. Amplification of rocking due to horizontal ground motion. *Earthquake Spectra*. 2012;28(4):1405–1421. https://doi.org/10.1193/1.4000085
3. Casapulla C & Maione A. A Simplified Equation of Motion for Free Rocking Rigid Blocks. Pp. 120–26 In: Insights and Innovations in Structural Engineering, Mechanics and Computation - Proceedings of the 6th International Conference on Structural Engineering, Mechanics and Computation, SEMC 2016.
4. Casapulla C, Maione A. Free damped vibrations of rocking rigid blocks as uniformly accelerated motions. *Int J Struct Stab Dyn*. 2016;17(6):1–19.
5. NTC2018. Italian Technical Standards for Buildings (Nuove Norme Tecniche per le Costruzioni, in Italian), Decreto Ministeriale 17/01/2018. 2018.
6. Housner GW. The behavior of inverted pendulum structures during earthquakes. *Bull Seismol Soc Am*. 1963;53(2):403–417. https://doi.org/10.1017/CBO9781107415324.004
7. Lipscombe PR, Pellegrino S. Free rocking of prismatic blocks. *J Eng Mech*. 1993;119(7):1387–1410. https://doi.org/10.1061/(ASCE)0733-9399(1993)119:7(1387)
8. Sorrentino L, AlShawa O, Decanini LD. The relevance of energy damping in unreinforced masonry rocking mechanisms. Experimental and analytic investigations. *Bull Earthquake Eng*. 2011;9(5):1617–1642. https://doi.org/10.1007/s10518-011-9291-1
9. Giresini L, Sassu M. Horizontally restrained rocking blocks: evaluation of the role of boundary conditions with static and dynamic approaches. *Bull Earthquake Eng*. 2017;15(1):385–410. https://doi.org/10.1007/s10518-016-9967-7
10. Giresini L, Fragiacomo M, Sassu M. Rocking analysis of masonry walls interacting with roofs. *Eng Struct*. 2016;116:107–120.
11. Mauro A, Felice dG, DeJong MJ. The relative dynamic resilience of masonry collapse mechanisms. *Eng Struct*. 2015;85:182–194. https://doi.org/10.1016/j.engstruct.2014.11.021
12. Aghagholizadeh M, Makris N. Earthquake response analysis of yielding structures coupled with vertically restrained rocking walls. *Earthquake Engineering & Structural Dynamics*. 2018;47 (15):2965–2984. https://doi.org/10.1002/eqe.3116
13. Solarino F, Giresini L & Oliveira DV Mitigation of amplified response of restrained rocking walls through horizontal dampers. In: Papadrakakis M, Fragiadakis M, Papadimitiou C. eds. EURODYN 2020 - XI International Conference on Structural Dynamics. Athens, Greece: 2020.
14. Dimitrakopoulos EG, DeJong MJ. Overturning of retrofitted rocking structures under pulse-type excitations. *J Eng Mech*. 2012;138(8):963–972. https://doi.org/10.1061/(ASCE)EM.1943-7889.0000410
15. Calderini C, Vecchiattini R, Battini C & Piccardo P Mechanical and metallographic characterization of iron tie-rods in masonry buildings: an experimental study. In: Van Balen & Verstrynge. ed. Structural Analysis of Historical Constructions: Anamnesis, diagnosis, therapy, controls - Proceedings of the 10th International Conference on Structural Analysis of Historical Constructions, SAHC 2016. London: Taylor & Francis Group; 2016:1293–1300.
16. Casapulla C, Argiento LU. The comparative role of friction in local out-of-plane mechanisms of masonry buildings. Pushover analysis and experimental investigation. *Eng Struct*. 2016;126:158–173. https://doi.org/10.1016/j.engstruct.2016.07.036
17. AlShawa O, Liberatore D, Sorrentino L. Dynamic one-sided out-of-plane behavior of unreinforced-masonry wall restrained by elasto-plastic tie-rods. *Int J Architect Heritage*. 2019;00(00):1–18. https://doi.org/10.1080/15583058.2018.1563226
18. Giresini L, Casapulla C, Denysiuk R, Matos J, Sassu M. Fragility curves for free and restrained rocking masonry façades in one-sided motion. *Eng Struct*. 2018;164:195–213. https://doi.org/10.1016/j.engstruct.2018.03.003
19. Bradley BA. A comparison of intensity-based demand distributions and the seismic demand hazard for seismic performance assessment. *Earthquake Eng Struct Dyn*. 2013. https://doi.org/10.1002/eqe
20. Abrams DP, AlShawa O, Lourenço PB, Sorrentino L. Out-of-plane seismic response of unreinforced masonry walls: conceptual discussion, research needs, and modeling issues. *Int J Architect Heritage*. 2017. https://doi.org/10.1080/15583058.2016.1238977
21. C.S.LL.PP. Circolare 21 gennaio 2019 n.7 Istruzioni per l'applicazione dell'Aggiornamento delle Norme tecniche per le costruzioni di cui al decreto ministeriale 17 gennaio 2018. 2019.
22. Giresini L, Solarino F, Taddei F, Mueller G. Experimental estimation of energy dissipation in rocking masonry walls restrained by an innovative seismic dissipator (LICORD). *Bull Earthquake Eng*. 2021. https://doi.org/10.1007/s10518-021-01056-6
23. Tomaževič M, Lutman M, Weiss P. Seismic upgrading of old brick-masonry urban houses: Tying of walls with steel ties. *Earthquake Spectra*. 1996;12(3):599–622. https://doi.org/10.1193/1.1585898
24. Degli Abbati S, Cattari S, Lagomarsino S. Theoretically-based and practice-oriented formulations for the floor spectra evaluation. *Earthquakes Struct*. 2018;15(5):000–000.
25. Dimitrakopoulos EG, Paraskeva TS. Dimensionless fragility curves for rocking response to near-fault excitations. *Earthquake Eng Struct Dyn*. 2015;44(12):2015–2033. https://doi.org/10.1002/eqe.2571
26. Baker JW. Efficient analytical fragility function fitting using dynamic structural analysis. *Earthquake Spectra*. 2015. https://doi.org/10.1193/021113EQS025M
27. Ibarra LF, Krawinkler H. Global Collapse of Frame Structures under Seismic Excitations. tech. rep., 2005.
28. Porter K, Kennedy R, Bachman R. Creating fragility functions for performance-based earthquake engineering. *Earthquake Spectra*. 2007. https://doi.org/10.1193/1.2720892

29. Bradley BA, Dhakal RP. Error estimation of closed-form solution for annual rate of structural collapse. *Earthquake Eng Struct Dyn*. 2008. https://doi.org/10.1002/eqe.833

30. Luzi L, Puglia R, Russo E, et al. The engineering strong-motion database: A platform to access pan-European accelerometric data. *Seismol Res Lett*. 2016. https://doi.org/10.1785/0220150278

31. Trifunac MD, Brady AG. A study on the duration of strong earthquake ground motion. *Bull Seismol Soc Am*. 1975;65(3):581–626. https://doi.org/10.1016/0148-9062(76)90487-3

32. Psycharis IN, Fragiadakis M, Stefanou I. Seismic reliability assessment of classical columns subjected to near-fault ground motions. *Earthquake Eng Struct Dyn*. 2013;42(14):2061–2079. https://doi.org/10.1002/eqe.2312

33. Padgett JE, Nielson BG, DesRoches R. Selection of optimal intensity measures in probabilistic seismic demand models of highway bridge portfolios. *Earthquake Eng Struct Dyn*. 2008;37(5):711–725. https://doi.org/10.1002/eqe.782

34. Watson-Lamprey J, Abrahamson N. Selection of ground motion time series and limits on scaling. *Soil Dyn Earthquake Eng*. 2006. https://doi.org/10.1016/j.soildyn.2005.07.001

35. Giresini L, Fragiacomo M, Lourenço PB. Comparison between rocking analysis and kinematic analysis for the dynamic out-of-plane behavior of masonry walls. *Earthquake Eng Struct Dyn*. 2015;44(13):2359–2376. https://doi.org/10.1002/eqe.2592

36. Jalayer F, Cornell CA. Alternative non-linear demand estimation methods for probability-based seismic assessments. *Earthquake Eng Struct Dyn*. 2009(38):951–972. https://doi.org/10.1002/eqe.876

37. Baker JW, Cornell CA. A vector-valued ground motion intensity measure consisting of spectral acceleration and epsilon. *Earthquake Eng Struct Dyn* 2005. https://doi.org/10.1002/eqe.474

38. Casapulla C, Jossa P, Maione A. Rocking motion of a masonry rigid block under seismic actions: A new strategy based on the progressive correction of the resonance response. *Ingegneria Sismica*. 2010;27(4):35–48.

39. Casapulla C, Maione A. Critical response of free-standing rocking blocks to the intense phase of an earthquake. *Int Rev Civil Eng*. 2017;8(1):1–10.